Journal of Anatomy

J. Anat. (2016) doi: 10.1111/joa.12449

REVIEW ARTICLE

Diffusible iodine-based contrast-enhanced computed tomography (diceCT): an emerging tool for rapid, high-resolution, 3-D imaging of metazoan soft tissues

Paul M. Gignac,[1] Nathan J. Kley,[2] Julia A. Clarke,[3] Matthew W. Colbert,[3] Ashley C. Morhardt,[4] Donald Cerio,[4] Ian N. Cost,[5] Philip G. Cox,[6] Juan D. Daza,[7] Catherine M. Early,[4] M. Scott Echols,[8] R. Mark Henkelman,[9] A. Nele Herdina,[10] Casey M. Holliday,[5] Zhiheng Li,[3] Kristin Mahlow,[11] Samer Merchant,[12] Johannes Müller,[11] Courtney P. Orsbon,[13] Daniel J. Paluh,[14] Monte L. Thies,[7] Henry P. Tsai[5,15] and Lawrence M. Witmer[16]

[1]*Department of Anatomy and Cell Biology, Oklahoma State University Center for Health Sciences, Tulsa, OK, USA*
[2]*Department of Anatomical Sciences, Stony Brook University, Stony Brook, NY, USA*
[3]*Department of Geological Sciences, Jackson School of Geosciences, The University of Texas at Austin, Austin, TX, USA*
[4]*Department of Biological Sciences, Ohio University, Athens, OH, USA*
[5]*Department of Pathology and Anatomical Sciences, University of Missouri, Columbia, MO, USA*
[6]*Department of Archaeology, University of York and Hull York Medical School, York, UK*
[7]*Department of Biological Sciences, Sam Houston State University, Huntsville, TX, USA*
[8]*The Medical Center for Birds, Oakley, CA, USA*
[9]*Department of Medical Biophysics, University of Toronto, Toronto, ON, Canada*
[10]*Department of Theoretical Biology, University of Vienna, Vienna, Austria*
[11]*Museum für Naturkunde, Leibniz-Institut für Evolutions- und Biodiversitätforschung an der Humboldt-Universität zu Berlin, Berlin, Germany*
[12]*Department of Biomedical Engineering, The University of Utah, Salt Lake City, UT, USA*
[13]*Department of Organismal Biology and Anatomy, The University of Chicago, Chicago, IL, USA*
[14]*Department of Biology, Villanova University, Villanova, PA, USA*
[15]*Department of Ecology and Evolutionary Biology, Brown University, Providence, RI, USA*
[16]*Department of Biomedical Sciences, Ohio University, Athens, OH, USA*

Abstract

Morphologists have historically had to rely on destructive procedures to visualize the three-dimensional (3-D) anatomy of animals. More recently, however, non-destructive techniques have come to the forefront. These include X-ray computed tomography (CT), which has been used most commonly to examine the mineralized, hard-tissue anatomy of living and fossil metazoans. One relatively new and potentially transformative aspect of current CT-based research is the use of chemical agents to render visible, and differentiate between, soft-tissue structures in X-ray images. Specifically, iodine has emerged as one of the most widely used of these contrast agents among animal morphologists due to its ease of handling, cost effectiveness, and differential affinities for major types of soft tissues. The rapid adoption of iodine-based contrast agents has resulted in a proliferation of distinct specimen preparations and scanning parameter choices, as well as an increasing variety of imaging hardware and software preferences. Here we provide a critical review of the recent contributions to iodine-based, contrast-enhanced CT research to enable researchers just beginning to employ contrast enhancement to make sense of this complex new landscape of methodologies. We provide a detailed summary of recent case studies, assess factors that govern success at each step of the specimen storage, preparation, and imaging processes, and make recommendations for standardizing both techniques and reporting practices.

Correspondence
Paul M. Gignac, Department of Anatomy and Cell Biology, Oklahoma State University Center for Health Sciences, Tulsa, OK 74107, USA. T: + 1 918 5618265; E: paul.gignac@okstate.edu

Accepted for publication *5 January 2016*

Finally, we discuss potential cutting-edge applications of diffusible iodine-based contrast-enhanced computed tomography (diceCT) and the issues that must still be overcome to facilitate the broader adoption of diceCT going forward.

Key words: alcoholic iodine; destaining; Lugol's iodine; radiographic contrast agents; three-dimensional imaging; X-ray micro-CT scanning.

Introduction

From the earliest light microscopy to the most recent innovations in synchrotron X-ray imaging, the introduction and advancement of visualization techniques have greatly improved and refined our knowledge about the composition and organization of biological systems. In each case, advances in imaging have facilitated significant discoveries that had once been thought unattainable. Visualization techniques used by morphologists, for example, have traditionally included such approaches as serial histological sectioning and photomicroscopy, wax-plate reconstructions, and gross dissection, each of which is time-consuming and ultimately destructive to the tissues under examination. More recently, non-destructive visualization techniques have come to the forefront, including X-ray computed tomography (CT), magnetic resonance imaging (MRI), selective plane illumination microscopy (SPIM), and optical projection tomography (OPT). These tools have allowed for effective data acquisition and anatomical visualization across a broad range of tissue types, specimens, and sizes, with CT being excellent for imaging mineralized tissues (e.g. bone, dentin, enamel) in particular, MRI providing good soft-tissue imaging, SPIM being capable of high-resolution time-lapse documentation of developmental processes in whole embryos, and OPT being especially well suited to visualizing patterns of gene expression.

Investments by academic and medical institutions, as well as those by government agencies, have helped increase access among researchers to core radiology facilities in both the developed and developing world. As a result of these efforts, and the growth of web-accessible digital repositories (e.g. DigiMorph, MorphoBank, Dryad), morphological studies that harness X-ray imaging techniques [including both standard CT and micro-CT (μCT)] have far surpassed those of other non-destructive visualization methods (Neu & Genin, 2014). The increasing availability of these resources has encouraged medical professionals and other researchers to develop innovative means to utilize X-ray imaging to document non-mineralized soft-tissue structures that typically do not image well using conventional X-ray techniques. Their approaches have focused primarily on the use of contrast-enhancing staining agents that increase the radiodensities of certain soft tissues so that the quality of their visualization in CT is comparable to (or even far greater than) that of naturally mineralized tissues (Wallingford, 1953; Harris et al., 1979; Webb et al. 2005). Additionally, results obtained using such radiographic contrast agents have been shown to be comparable to those using MRI (de Crespigny et al. 2008), which is typically considered to be a somewhat less accessible technique for reasons of cost and availability. Currently, several contrast agents are used by researchers for their soft-tissue specificity and radiopacity: iodine [dissolved in ethanol (I_2E), methanol (I_2M), or water (I_2KI, or Lugol's solution); Metscher, 2009a,b; Degenhardt et al. 2010], osmium tetroxide (OsO_4; Metscher, 2009a,b; Mizutani & Suzuki, 2012; Pauwels et al. 2013), phosphomolybdic acid (PMA; Pauwels et al. 2013), and phosphotungstic acid (PTA; Metscher, 2009a,b; Pauwels et al. 2013). (For additional staining agents and imaging comparisons, see 'Other contrast agents' below.) As a result, contrast-enhanced X-ray images, particularly in the form of 3-D CT image stacks, have facilitated high-fidelity studies of soft-tissue organization, arrangement, and morphometrics at increasing levels of detail (e.g. micrometer and nanometer scales) that were not possible even a decade ago.

Lugol's iodine, also known as Strong solution or iodine-potassium iodide (I_2KI) – an aqueous solution consisting of two parts KI for every one part I_2 – has gained the strongest following among descriptive anatomists and functional morphologists as an effective contrast agent for its relative ease of handling, cost effectiveness, and differential affinities for major types of soft tissues. Metscher (2009a,b) popularized Lugol's iodine as a diffusible contrast agent for 3-D visualization of soft tissues using standard μCT imaging approaches by comparing scans of invertebrates, vertebrate embryos, and small hatchling specimens stained with I_2KI and other contrast-enhancing solutions. Expanding on this seminal work and seeking to better visualize soft tissues within their own study organisms, other researchers began exploring a broader range of animal specimens, tissue types, and staining protocols to provide detailed anatomical interpretations bearing on ongoing medical, systematic, developmental, and functional morphological research in a broad array of invertebrates (Jaspers & Carstensen, 2009; Faulwetter et al. 2013; Fernández et al. 2014; Lenihan et al. 2014; Akkari et al. 2015), additional vertebrate embryos (Wong et al. 2012), and in a wide variety of post-embryonic bony fishes (Metscher, 2013; Kleinteich et al. 2014), amphibians (Kleinteich & Gorb, 2015a,b), reptiles (Tsai & Holliday, 2011; George & Holliday, 2013; Holliday et al. 2013; Gignac & Kley, 2014; Tsai & Holliday, 2015), birds (Düring et al. 2013; Lautenschlager et al. 2013; Tahara & Larson, 2013; Gignac & Kley, 2014), and mammals (Degenhardt et al.

2010; Herdina et al. 2010; Tobita et al. 2010; Cox & Jeffery, 2011; Jeffery et al. 2011; Hautier et al. 2012; Stephenson et al. 2012; Aslanidi et al. 2013; Baverstock et al. 2013; Pauwels et al. 2013; Vickerton et al. 2013; Cox & Faulkes, 2014; Herdina et al. 2015a,b; Li & Clarke, in press). Exemplar images and 3-D renderings demonstrating the impressive taxonomic range and anatomical detail captured through use of this approach are illustrated in Figs 1 and 2. Pursuing distinct research goals, various studies have also sought to optimize iodine staining techniques for numerous tissue- and protocol-specific situations, including neurological visualizations (Metscher, 2013; Gignac & Kley, 2014), muscle imaging and measurement (at the levels of whole muscles, individual fascicles, and gross fiber types; Cox & Jeffery,

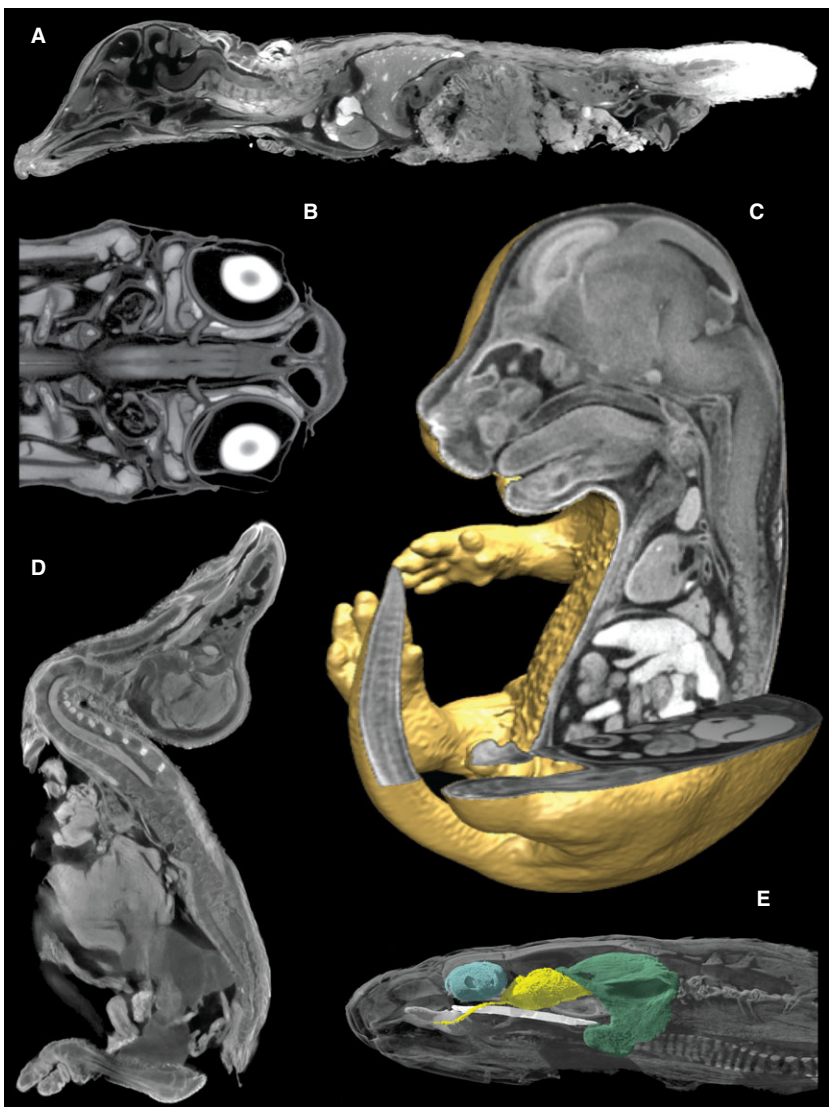

Fig. 1 A phylogenetically and morphologically diverse sample of tetrapods imaged using diffusible iodine-based contrast-enhanced computed tomography (diceCT), demonstrating the diversity of soft tissue types (e.g. muscles, glands, nerves, epithelia, fat) that can be visualized using this technique. (A) Sagittal slice through a crocodylian hatchling [*Alligator mississippiensis* (American alligator)], showing that Lugol's iodine solution readily penetrates even the heavily keratinized integument of reptiles, allowing for the clear visualization of internal organs such as the brain, heart, and liver. (B) Frontal slice through the head of an adult amphibian [*Rana sylvatica* (wood frog)], illustrating the detailed anatomical relationships among small, intricate structures of the auditory and ocular systems. (C) Sagittal and transverse biplanar cutaway view of a 3-D volume rendering of a mammal [*Mus musculus* (house mouse)] embryo (15.5 days), showing the clarity with which minute developing structures can be imaged using diceCT. (D) Sagittal slice through a hatchling bird [*Tyto alba* (barn owl)], showing the completeness of whole-body staining for post-embryonic specimens. (E) Sagittal cutaway view of a 3-D volume rendering of the head of an adult snake [*Vipera berus* (European adder)], showing digital reconstructions of the eye (blue), venom gland (yellow), ectopterygoid bone (white), and jaw adductor musculature (green). Specimens not to scale. Specimen preparation, staining, and scanning parameters can be found in Tables 1 and S1. Specimen images contributed by A.C.M., C.M.E., J.M., K.M., L.M.W., N.J.K., P.M.G., and R.M.H.

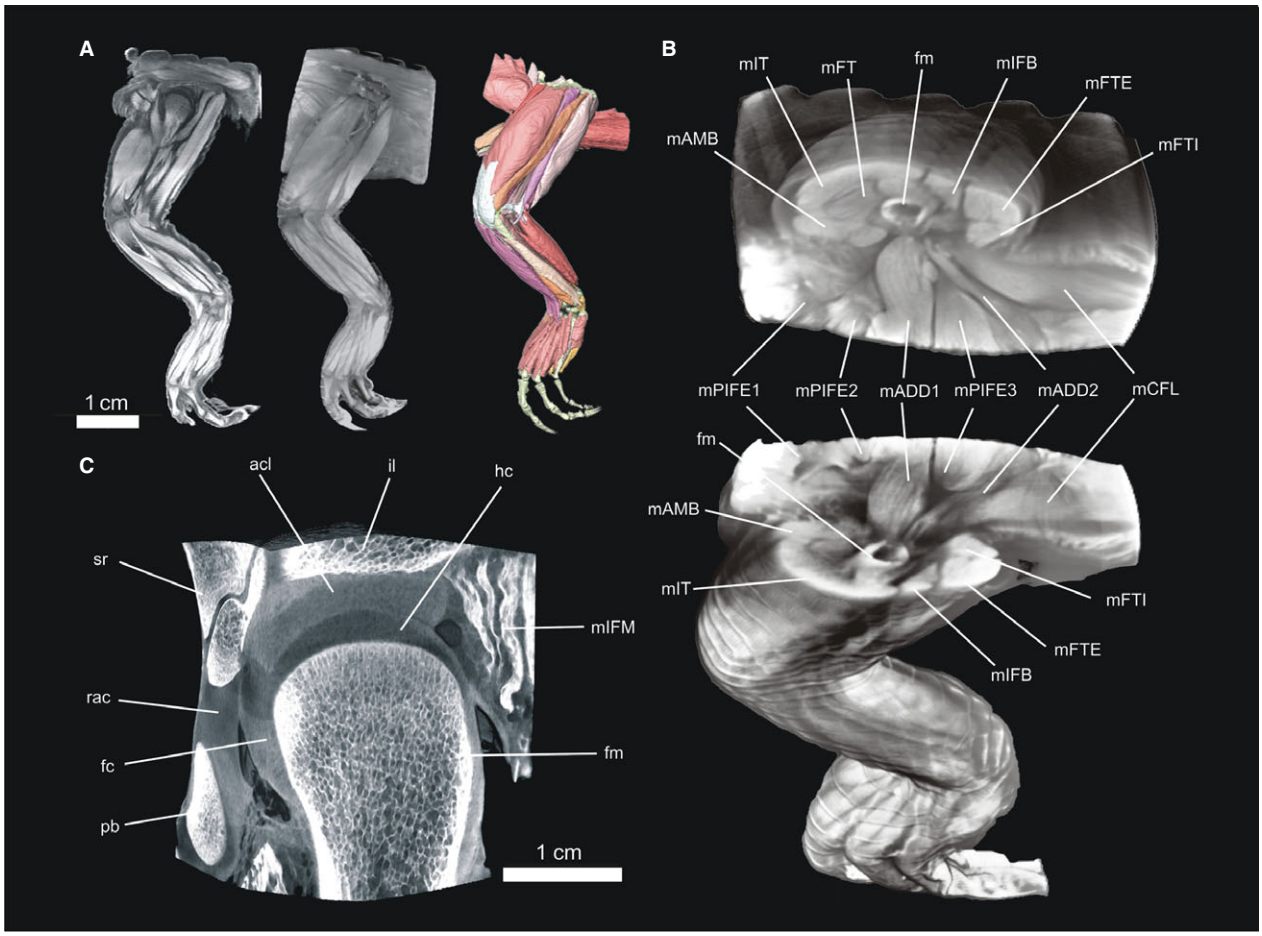

Fig. 2 DiceCT imaging of American alligator (*Alligator mississippiensis*) hind limbs. (A) A 2-D section through the acetabulum of a juvenile specimen (left), which was rendered into a single volume based on grayscale values (middle) and used as the basis for individually reconstructing limb muscles and bony elements in three dimensions (right). (B) A volumetric representation of a juvenile hind limb, sectioned through the proximal femoral metaphysis, demonstrating muscle bellies from ventral (top) and dorsal (bottom) views. (C) A close-up view of the hip joint in an adult specimen, sectioned into an oblique anterolateral view and demonstrating acetabular soft tissues and oblique cartilages. acl, acetabular labrum; fc, fibrocartilage; fm, femur; hc, hyaline cartilage; il, ilium; mADD, m. adductor femoralis (parts 1 and 2); mAMB, m. ambiens; mCFB, m. caudofemoralis brevis; mCFL, m. caudofemoralis longus; mFT, m. femorotibialis; mFTE, m. flexor tibialis externus; mFTI, m. flexor tibialis internus; mIFB, m. iliofibularis; mIFM, m. iliofemoralis; mIT, m. iliotibialis; mPIFE, m. puboischiofemoralis externus (parts 1–3); pb, pubis; rac, rostral acetabular cartilage; sr, sacral rib. Specimen preparation, staining, and scanning parameters can be found in Tables 1 and S1. Specimen images contributed by C.M.H. and H.P.T.

2011; Tsai & Holliday, 2011; Düring et al. 2013; Holliday et al. 2013; Lautenschlager et al. 2013; Gignac & Kley, 2014), comparisons with histological preparations (Jeffery et al. 2011; Herdina et al. 2015b), size-related exposure to iodine (Gignac & Kley, 2014), 3-D rendering automation (Dechamps et al. 2014), and staining artifacts such as shrinkage (Pauwels et al. 2013; Vickerton et al. 2013; Wong et al. 2013).

The collective result of these studies is a complex landscape of highly varied approaches that differ in specimen preparation, iodine staining protocols, CT hardware, imaging parameters, 3-D reconstruction software, and reporting practices. To make sense of this new landscape, especially for researchers who are new to contrast-enhanced imaging, a comprehensive evaluation of these myriad contributions and an assessment of the current state of the science are required. Our goal in this paper is to provide such a synthesis. This overview represents the experiences, opinions, and consensus that emerged from the Austin Working Group, 'Advancing contrast-enhanced CT imaging in the biological sciences' [held at The University of Texas (UT) at Austin, 2–3 April 2015; organized by P.M.G., N.J.K., J.A.C., M.W.C., and A.C.M., and supported by UT, The UTCT Laboratory, and the National Science Foundation (NSF EAGER 1450850 and 1450842 awarded to P.M.G. and N.J.K., respectively)].

Because of the variety of variables that influence the effectiveness of diffusible iodine-based contrast-enhanced computed tomography (diceCT), there is no singular protocol that we can recommend for all specimens, researcher interests or desired visualization outcomes. Instead, our

goals are focused on making this emerging tool more accessible for the broadest range of morphological researchers at the widest range of institutions. To that end, this paper will: (1) provide a summary of recent case studies from the scientific literature and synthesize the elements of successful approaches; (2) analyze factors that govern success at each step of the specimen storage, preparation, and imaging processes, as well as provide general recommendations based on the literature and the collective experience of the authors; (3) recommend a standard for reporting details of specimens preparation, storage, and imaging that will be pivotal to the repeatability and broader adoption of diceCT going forward; and (4) discuss cutting-edge applications and future directions for diceCT techniques based on the range of existing published studies as well as ongoing research.

Case studies and recommendations

More than two dozen studies have been published over the last seven years, using various elements of the diceCT approach summarized in this paper (see Table 1). These have been based on nearly 100 specimens, collectively representing impressively broad phylogenetic and developmental samples of metazoans. Some of these studies sought specifically to further develop and/or refine contrast-enhanced CT imaging techniques, whereas others aimed to demonstrate and describe important anatomical features of targeted study taxa. Tables 1 and Supporting Information Table S1 catalogue these studies and include some parameters and details that were not previously published in the cited articles. These tables also give a sense of the breadth of iodine-enhanced μCT research. In this case study section, we assess patterns of technique effectiveness for studies varying in specimen type, staining, and μCT imaging, and we refer to specific case studies presented in these tables in our discussion below. Table S1 is provided so that readers can sort data from these studies by variables relating to specimen preparation, staining, and scanning.

Specimen type

Twelve classes of metazoans have been imaged successfully thus far using these techniques: Actinopterygii, Amphibia, Aves, Cephalopoda, Chilopoda, Clitellata, Diplopoda, Hyperoartia, Insecta, Mammalia, Polychaeta, and Reptilia (Table 1). From isolated anatomical structures of interest (e.g. head, heart, limbs, syrinx) to whole embryonic and adult organisms, researchers have successfully applied these techniques across more than 10 000-fold differences in specimen size. Metazoan soft tissues are highly amenable to contrast enhancement using iodine-based solutions across a broad range of developmental stages, integumentary compositions, positions within the body, locations within anatomical compartments (e.g. cranial cavity), and histological tissue types. One notable exception is hyaline cartilage, which is stained poorly by iodine. Nonetheless, cartilaginous structures can be distinguished indirectly by the perichondria surrounding them, which stains readily using iodine-based solutions. It is remarkable – and speaks to the broad utility of iodine – that over the last several years these techniques have spread so rapidly (see Table 1). As technologies improve, the resolution, power, and gantry capacities of CT scanners will doubtless continue to increase. It is, therefore, likely that scientists will be able to continue adding to this wide range of taxa for years to come.

Specimen treatment

Fixation

As a general recommendation, we urge researchers to prepare for fixation the freshest possible tissues in order to maximize the quality of the specimens sampled and, thus, the image data derived from them. However, several studies have been successful using museum specimens or those initially collected for purposes other than contrast-enhanced imaging (e.g. Herdina et al. 2010; Cox & Jeffery, 2011; Jeffery et al. 2011; Cox & Faulkes, 2014; Herdina et al. 2015a,b). Nonetheless, specimen treatments, including freezing prior to fixation, choice of fixation agent, and fixation process, can significantly affect staining outcomes (see details in 'Reporting standards' below). We also urge researchers to sample for potential DNA analyses prior to treatments, if genetic research needs are anticipated. Although fixative likely has a larger impact on the effectiveness of DNA extraction and amplification, the impact of iodine staining on the structural integrity of DNA is currently unknown.

Specimens should be fixed thoroughly prior to staining and imaging (see Fig. 3). Numerous fixatives have been used for this purpose: Bouin's solution (Metscher, 2009a; Sombke et al. 2015), Dent's solution (Metscher, 2009a), Duboscq-Brasil solution (Sombke et al. 2015), 70–95% solutions of ethanol (Herdina et al. 2010; Fernández et al. 2014; Kleinteich et al. 2014), 2.5% glutaraldehyde (Metscher, 2009b; Sombke et al. 2015), 4–10% phosphate-buffered formalin solutions (Metscher, 2009a,b; Cox & Jeffery, 2011; Jeffery et al. 2011; Tsai & Holliday, 2011; Aslanidi et al. 2013; Baverstock et al. 2013; George & Holliday, 2013; Holliday et al. 2013; Lautenschlager et al. 2013; Gignac & Kley, 2014; Tsai & Holliday 2015; Herdina et al. 2015a), and 4% paraformaldehyde (Metscher, 2009a; Degenhardt et al. 2010; Wong et al. 2012). Personal preferences, availability, cost, potential for specimen shrinkage, and potential impact on future DNA work will likely all factor into a researcher's choice(s) of fixative.

There is no single ideal fixative. Those that have been used commonly in prior contrast-enhanced imaging research have long histories of effective use for the general fixation of both vertebrate and invertebrate specimens

Table 1 Taxonomic affinities, developmental stages, staining parameters, and select scanner settings reported in the iodine-based contrast-enhanced μCT imaging literature. Extended documentation of specimen preparation and imaging settings can be found in Table S1, including specimen storage, fixation, μCT scanner models, and image-enhancement techniques, among other details. Table S1 is intended to help readers manipulate and contrast various aspects of specimen affinities, sizes, preparation regimes, and μCT scanning parameters, as well as to identify specimen images already available in the literature that may match a researcher's similar imaging needs.

Reference(s)	Taxon	Ontogenetic status	Anatomical region	Stain agent	Stain % w/v	Staining duration	μA	kVp
[1]	*Ommatoiulus avatar* (Diplopoda)	Adult	Anterior body	I_2E	1%	Overnight	–	60
[1]	*Ommatoiulus avatar* (Diplopoda)	Adult	Genital region (male)	I_2E	1%	Overnight	–	60
[1]	*Ommatoiulus avatar* (Diplopoda)	Adult	Anterior body	I_2E	1%	Overnight	–	60
[2]	*Canis familiaris* (Mammalia)	Adult (8 yr old)	Heart	I_2KI	5–10%	4–7 days	–	150
[3]	*Mus musculus* (Mammalia)	Adult	Head	I_2KI	3.75%	1 week	105	75
[4]	*Heterocephalus glaber* (Mammalia)	Adult	Head	I_2KI	5%	2 weeks	60	80
[5, 6, 7]	*Sciurus carolinensis* (Mammalia)	Adult	Head	I_2KI	25%	7 weeks	110	195
[5, 6, 7]	*Cavia porcellus* (Mammalia)	Adult	Head	I_2KI	25%	7 weeks	99	215
[5, 6, 7]	*Rattus norvegicus* (Mammalia)	Adult	Head	I_2KI	25%	2 weeks	90	100
[8]	*Mus musculus* (Mammalia)	Embryos (E10.5, E11.5, E13.5, E15.5, E17.5) and postnatal specimens (PN0)	Whole	I_2KI	10.58%	24/48/72 h	80	80
[9]	*Lygaeus simulans* (Insecta)	Adult	Whole	I_2E	1.00%	4 days	190	105
[10]	*Taeniopygia guttata* (Aves)	–	Whole	I_2KI	0.10%	2 days	110	85
[11]	*Eunice* sp. (Polychaeta)	Juvenile	Whole	I_2E	1%	24 h	167	60
[11]	*Syllis gracilis* (Polychaeta)	–	Anterior end and mid-body	I_2E	1%	3 days	167	60
[12]	*Aporrectodea caliginosa* (Clitellata)	–	Whole	I_2KI	10%	4 days	100	65
[12]	*Aporrectodea caliginosa* (Clitellata)	–	Whole	I_2KI	10%	10 days	100	65
[13]	*Alligator mississippiensis* (Reptilia)	Neonate	Head	I_2KI	11.25%	2 weeks	135	200
[13]	*Alligator mississippiensis* (Reptilia)	Subadult	Head	I_2KI	11.25%	4 weeks	145	160
[13, 14]	*Dromaius novaehollandiae* (Aves)	Juvenile	Head	I_2KI	11.25%	4 weeks	130	190
[15]	*Proechimys cuvieri* (Mammalia)	Adult	Head	I_2KI	10%	1 week	–	–
[16]	*Plecotus austriacus* (Mammalia)	Adult	Penis	I_2KI, I_2E	1%, 1%	Overnight or days to ~ 2 weeks	43	79
[17]	*Nyctalus noctula* (Mammalia)	Adult	Penis	I_2E	1%	Overnight or days to ~ 2 weeks	67–200	40–60
[17]	*Pipistrellus pipistrellus* (Mammalia)	Adult	Penis	I_2E	1%	Overnight or days to ~ 2 weeks	67–200	40–60

(continued)

Table 1 (continued)

Reference(s)	Taxon	Ontogenetic status	Anatomical region	Stain agent	Stain % w/v	Staining duration	μA	kVp
[17]	*Pipistrellus nathusii* (Mammalia)	Adult	Penis	I_2E	1%	Overnight or days to ~ 2 weeks	67–200	40–60
[18]	*Pipistrellus pipistrellus* (Mammalia)	Juvenile	Penis	I_2E	1%	Overnight or days to ~ 2 weeks	67–200	40–60
[19]	*Rattus norvegicus* (Mammalia)	Adult	Sciatic nerve	I_2KI	6%	48 h	300	80
[20]	*Homo sapiens* (Mammalia)	Fetus	Heart	I_2KI	6.33%	48 h	50–135	85–125
[21]	*Mus musculus* (Mammalia)	Adult	Head	I_2KI	2.25%	7 h	100	77
[21]	*Mus musculus* (Mammalia)	Adult	Head	I_2KI	3.75%	7 h	105	75
[21]	*Mus musculus* (Mammalia)	Adult	Head	I_2KI	3.75%	7 h	105	75
[21]	*Mus musculus* (Mammalia)	Adult	Head	I_2KI	7.50%	1 day	100	75
[21]	*Sciurus carolinensis* (Mammalia)	Adult	Head	I_2KI	25%	48 days	110	195
[21]	*Sus scrofa scrofa* (Mammalia)	Fetus	Extensor digitorum longus muscle	I_2KI	15%	2 days	105	80
[22]	*Gobiesox maeandricus* (Actinopterygii)	–	–	I_2KI	1%	24 h	100	100
[22]	*Gobiesox maeandricus* (Actinopterygii)	–	–	I_2KI	1%	8 days	100	100
[23]	*Bombina variegata* (Amphibia)	Adult	Whole	I_2KI	–	–	100	100
[23, 24]	*Ceratophrys ornata* (Amphibia)	Adult	Whole	I_2KI	4%	2 weeks	100	100
[23, 24]	*Ceratophrys ornata* (Amphibia)	Adult	Tongue	I_2KI	4%	Overnight	140, 250	70, 40
[25]	*Buteo buteo* (Aves)	Adult	Head	I_2KI	10%	1 week	60	95
[26]	*Esox lucius* (Actinopterygii)	Neonate	Whole	I_2KI	0.30%	Overnight	200	30
[26]	*Lampetra* sp. (Hyperaortia)	Juvenile	Anterior portion	I_2E	1%	Overnight	160	50
[26]	*Polyodon spathula* (Actinopterygii)	Neonate	Head	I_2M	1%	Overnight	133	80
[26]	*Acipenser medirostris* (Actinopterygii)	–	Appendage	I_2M	1%	Overnight	200	40
[26]	*Xenopus* sp. (Amphibia)	Embryo (Nieuwkoop & Faber stage ca.27)	Whole	I_2KI	1%	Overnight	133	60
[26]	*Mus musculus* (Mammalia)	Embryo (Theiler stage 21)	Whole	I_2KI	1%	Overnight	100	80
[26]	*Sisyra* sp. (Insecta)	Adult	Whole	I_2E	1%	Overnight	83	60
[26]	*Sisyra* sp. (Insecta)	Adult	Whole	I_2E	1%	Overnight	83	60
[26]	*Ideosepius pygmeus* (Cephalopoda)	Neonate	Whole	I_2KI	1%	Overnight	150	40

(continued)

Table 1 (continued)

Reference(s)	Taxon	Ontogenetic status	Anatomical region	Stain agent	Stain % w/v	Staining duration	μA	kVp
[27]	*Gallus gallus* (Aves)	Embryo (Hamburger & Hamilton stage 25)	Whole	I_2KI	0.30%	30 min	–	40
[27]	*Gallus gallus* (Aves)	Embryo (Hamburger & Hamilton stage 24)	Whole	I_2KI	0.30%	Overnight	–	40
[28]	*Sus domesticus* (Mammalia)	Adult	Isolated muscle and lipid tissue	KI	43%	24 h	–	120
[28]	*Mus musculus* (Mammalia)	Adult	Hind limb	KI	43%	24 h	–	120
[29]	*Mus musculus* (Mammalia)	Adult	Kidney, testicles, brain, liver, lungs, heart, stomach, and spleen	I_2E	1%	14 h	–	50, 70
[30]	*Scutigera coleoptrata* (Chilopoda)	–	Head	I_2E	1%	Overnight	200	20
[30]	*Scutigera coleoptrata* (Chilopoda)	–	Head	I_2E	1%	Overnight	200	20
[30]	*Vespa crabro* (Insecta)	Adult	Head	I_2E	1%	Overnight	200	30
[30]	*Vespa crabro* (Insecta)	Adult	Head	I_2E	1%	Overnight	200	30
[30]	*Lucilia* sp. (Insecta)	Adult	Head	I_2E	1%	Overnight	200	30
[30]	*Lucilia* sp. (Insecta)	Adult	Head	I_2E	1%	Overnight	200	30
[30]	*Lucilia* sp. (Insecta)	Adult	Head	I_2E	1%	Overnight	200	30
[30]	*Lucilia* sp. (Insecta)	Adult	Head	I_2E	1%	Overnight	200	30
[30]	*Lucilia sp.* (Insecta)	Adult	Head	I_2E	1%	Overnight	200	30
[30]	*Lucilia* sp. (Insecta)	Adult	Head	I_2E	1%	Overnight	200	30
[30]	*Lucilia* sp. (Insecta)	Adult	Head	I_2E	1%	Overnight	200	30
[30]	*Sarcophaga carnaria* (Insecta)	Adult	Head	I_2E	1%	Overnight	200	30
[30]	*Sarcophaga carnaria* (Insecta)	Adult	Head	I_2E	1%	Overnight	200	30
[30]	*Drosophila hydei* (Insecta)	Adult	Head	I_2E	1%	Overnight	200	30
[30]	*Drosophila hydei* (Insecta)	Adult	Head	I_2E	1%	Overnight	200	30
[31]	*Rattus domesticus* (Mammalia)	Adult	Heart	I_2KI	15%	2 days	120	145
[31]	*Rattus domesticus* (Mammalia)	Adult	Heart	I_2KI	7.50%	2 days	110	135
[31]	*Rattus domesticus* (Mammalia)	Adult	Heart	I_2KI	3.75%	2 days	115	130
[31]	*Rattus domesticus* (Mammalia)	Adult	Heart	I_2KI	1.87%	2 days	120	140
[31]	*Oryctolagus cuniculus* (Mammalia)	Adult	Heart	I_2KI	7.50%	3 days	150	155

(continued)

Table 1 (continued)

Reference(s)	Taxon	Ontogenetic status	Anatomical region	Stain agent	Stain % w/v	Staining duration	μA	kVp
[31]	*Oryctolagus cuniculus* (Mammalia)	Adult	Heart	I_2KI	3.75%	5 days	140	145
[31]	*Oryctolagus cuniculus* (Mammalia)	Adult	Heart	I_2KI	3.75%	5 days	120	135
[31]	*Oryctolagus cuniculus* (Mammalia)	Adult	Heart	I_2KI	7.50%	3 days	140	155
[32]	*Coturnix coturnix* (Aves)	Embryo (incubated for 15–16 days)	Whole	I_2KI	3.75%	2–28 days	80	80
[33]	*Mus musculus* (Mammalia)	Neonate	Whole	I_2KI	2.5% I_2/1.5% KI	96 h	–	–
[34, 35, 36]	*Alligator mississippiensis* (Reptilia)	Subadult	Head	I_2KI	10%	5 weeks	500	80
[37, 38]	*Alligator mississippiensis* (Reptilia)	Subadult	Hip joint	I_2KI	10%	~ 3–4 weeks	500	80
[39]	*Rattus norvegicus* (Mammalia)	Adult	Hind limb	I_2KI	9%	9 days	130	90
[40]	*Mus musculus* (Mammalia)	Embryo (E15.5)	Whole	I_2KI	1%	17 h	181	55
[41]	*Mus musculus* (Mammalia)	Embryo (E15.5)	Whole	I_2KI	1%	24 h	181	55
[41]	*Mus musculus* (Mammalia)	Embryo (E15.5)	Whole	I_2KI	4%	72 h	142	70
[38, 41]	*Mus musculus* (Mammalia)	Embryo (E15.5)	Whole	I_2KI	4%	24 h	142	79
[42]	*Mus musculus* (Mammalia)	Embryo (E15.5)	Whole	I_2KI	1%	24 h	100	100
[38]	*Alligator mississippiensis* (Reptilia)	Hatchling (PN0)	Whole	I_2KI	–	–	–	–
[38]	*Rana sylvatica* (Amphibia)	Adult	Head	I_2KI	5%	7 days	270	140
[38]	*Tyto alba* (Aves)	Neonate	Whole	I_2KI	5%	10 days	450	80
[38]	*Vipera berus* (Reptilia)	Adult	Head and neck	I_2KI	10, 20, then 40%	7, 100, then 7 days	150	50
[38]	*Crotalus atrox* (Reptilia)	Adult	Head	I_2KI	7.50%	21 days	180	140
[38]	*Ornithorhynchus anatinus* (Mammalia)	Adult	Head	I_2KI	7.50%	21 days	160	190
[38]	*Phasianus colchicus* (Aves)	Adult	Head	I_2KI	11%, then 6%	Over 2 months, then 2 weeks	83	120

I_2E, iodine dissolved in 100% ethanol; I_2KI, Lugol's Iodine; I_2M, iodine dissolved in 100% methanol; kVp, peak kilovoltage (often reported as kV); μA, micro-amperage.
References: [1] Akkari et al. (2015); [2] Aslanidi et al. (2013); [3] Baverstock et al. (2013); [4] Cox & Faulkes (2014); [5] Cox & Jeffery (2011); [6] Cox et al. (2011); [7] Cox et al. (2012); [8] Degenhardt et al. (2010); [9] Dougherty et al. (2015); [10] Düring et al. (2013); [11] Faulwetter et al. (2013); [12] Fernández et al. (2014); [13] Gignac & Kley (2014); [14] Balanoff et al. (2015); [15] Hautier et al. (2012); [16] Herdina et al. (2010); [17] Herdina et al. (2015a); [18] Herdina et al. (2015b); [19] Hopkins et al. (2015); [20] Hutchinson et al. (2016); [21] Jeffery et al. (2011); [22] Kleinteich et al. (2014); [23] Kleinteich & Gorb (2015a); [24] Kleinteich & Gorb (2015b); [25] Lautenschlager et al. (2013); [26] Metscher, 2009a; [27] Metscher (2009b); [28] Pauwels et al. (2013); [29] Silva et al. (2015); [30] Sombke et al. (2015); [31] Stephenson et al. (2012); [32] Tahara & Larson (2013); [33] Tobita et al. (2010); [34] Tsai & Holliday (2011); [35] Holliday et al. (2013); [36] George & Holliday (2013); [37] Tsai & Holliday (2015); [38] *this study*; [39] Vickerton et al. (2014); [40] Wong et al. (2012); [41] Wong et al. (2013); [42] Wong et al. (2014).

DiceCT Do's

- Fix specimens thoroughly for long-term stability before staining them in Lugol's iodine.
- Store Lugol's iodine solutions, specimens that are being stained, and previously stained specimens in amber glass or blacked-out containers to limit triiodide/iodide (I_3^-/I^-) redox reactions that degrade staining quality.
- Keep a stock solution of up to 5% sodium thiosulfate ($Na_2S_2O_3$) for destaining specimens and cleaning up lab spills.
- The specific regulations that govern disposal of iodine and iodide vary by state, province, region, and country. Check your institutional waste disposal policies regarding iodide. One option is to neutralize aqueous triiodide (I_3^-) into iodide (I^-) using sodium thiosulfate ($Na_2S_2O_3$), which may be easier to dispose of.

Fig. 3 DiceCT *Do's*: considerations and recommendations for successful specimen preparation.

(Humason, 1972). One general recommendation has been to limit specimen storage in ethanol between fixation and staining or, when storage is necessary, to store specimens in the same fluid fixatives as those that were used to fix the specimens originally. Lipids are soluble in alcohols (Jeffery et al. 1989) and this can be a problem for iodine-based stains. Namely, iodine appears to bind to lipids (Gignac & Kley, 2014), such as those present in myelinated nervous tissues. Reducing the lipid content of soft tissues will, therefore, reduce the amount of iodine that those tissues can hold. This, in turn, limits X-ray attenuation during CT scanning and overall contrast differences between lipid-dense and lipid-poor tissues. Figure 4A, an *Ornithorhynchus* specimen stored in 70% ethanol for more than 70 years, demonstrates this effect. Notably, however, some specimens in this condition can be contrasted enough to provide useful data and be manually rendered into 3-D digital datasets, depending on the condition of the specimen and the anatomical region(s) of interest. Unfortunately, any such effects on the image quality of a specimen likely will not be detectable until after the specimen has been CT-scanned.

Iodine staining

Whether staining specimens with I_2KI, I_2E or I_2M (see Fig. 5), four clear usage patterns appear across the relevant literature: (1) the vast majority of specimens have been stained with $\leq$ 1% weight/volume (w/v) iodine solutions ($\sim$ 60% of specimens in Table 1); (2) all specimens stained successfully with $>$ 1% aqueous elemental iodine solutions have been comparatively large (i.e. typical post-embryonic sizes; Table 1); (3) even for larger specimens, iodine solutions $>$ 10% have been used only relatively rarely (i.e. only $\sim$ 30% of tetrapod specimens in Table 1); and (4) with the exceptions of moderately sized specimens such as annelids (Faulwetter et al. 2013; Fernández et al. 2014) and vertebrate embryos secured in hydrogel (Wong et al. 2013), specimens stained for $>$ 24 h have been among the largest (Table 1). Thus, available data do not seem to suggest that any particular staining protocols should be favored over others based solely on the phylogenetic affinities of the specimens being examined. Rather, they suggest that

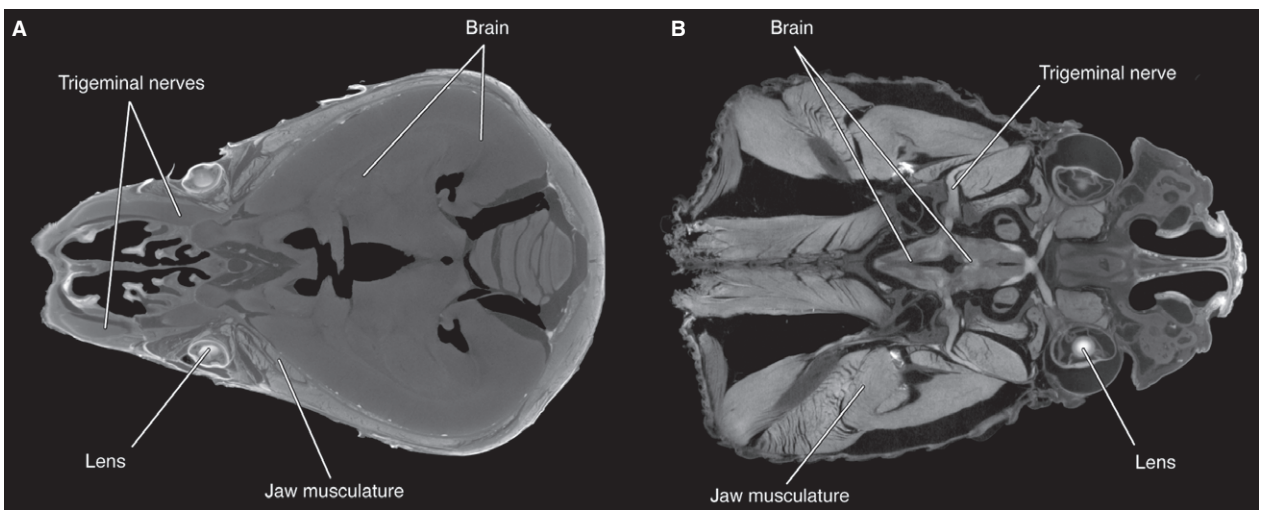

Fig. 4 Frontal diceCT slices through the heads of (A) a platypus (*Ornithorhynchus anatinus*; anterior to left) and (B) a western diamondback rattlesnake (*Crotalus atrox*; anterior to right). To ensure that both specimens are comparable, the grayscale ranges for A and B have been shifted so that the white values for the lenses (the whitest homologous structures of both specimens) are approximately equal. The platypus specimen was stored in 70% ethanol for more than 70 years and illustrates how the solubility of lipids in alcohol can reduce the potential for differentiation between different types of soft tissues in diceCT imaging of alcoholic specimens. In contrast, the rattlesnake was freshly fixed in 10% neutral buffered formalin, then stained and imaged shortly thereafter. Specimens are not to scale. Specimen preparation, staining, and scanning parameters can be found in Tables 1 and S1. Specimen images contributed N.J.K. and P.M.G..

DiceCT Don'ts

- Don't store your iodine anywhere near ammonia. These compounds can combine to form nitrogen triiodide (NI_3), which is a highly volatile contact explosive.
- Don't stain specimens in open containers. Evaporation from the staining solution will stain nearby lab space and equipment and alter the concentration of the staining solution.
- Don't overstain. Small specimens (≤ ~1 cm^3) can stain very quickly, so adjust staining times according to size to avoid overstaining. As a first step, reference the literature for similarly sized specimens (see Supplemental Table S1).
- For ethanol- and methanol-based iodine stains(I_2E, I_2M), don't use low-concentration alcohols. Staining is most effective when alcohol concentrations of 100% (or nearly so) are used.

Fig. 5 DiceCT *Don'ts*: situations to avoid for successful specimen preparation.

specimen size is the single most important consideration in dictating proper exposure to iodine staining.

In small specimens, iodine has absolutely shorter distances to travel to reach internal soft tissues. Thus, it is not surprising that smaller specimens require lower concentrations of I_2KI, I_2E, and I_2M, as well as shorter staining durations. In addition, solutions of higher concentrations exert higher osmotic pressures and, therefore, are taken up more quickly by soft tissues (Vickerton et al. 2013). Small specimens, such as most invertebrates and vertebrate embryos, can be stained at low concentrations (i.e. ≤ 1% w/v) for short durations (e.g. 'overnight') and still exhibit excellent levels of contrast when CT-scanned. For larger specimens, such as post-embryonic vertebrates, two approaches have generally been successful: low concentrations of staining solution (i.e. ≤ 1% w/v of I_2 in either an I_2KI or I_2E solution, approximately isotonic to vertebrate blood) refreshed regularly for long staining periods (i.e. several weeks to months; A.C.M. & A.N.H., pers. obs.) or higher concentrations of staining solution (up to ~ 10% w/v) for shorter durations (i.e. a few weeks; Gignac & Kley, 2014). Internal regions of interest are located considerably further away from the exposed external surfaces of these specimens. At the same time, these regions contain a proportionally higher volume of soft tissues relative to the surface area through which the iodine diffuses. Thus, both higher exposure to iodine ions through iterative refreshing of low concentrations and un-refreshed high concentrations seem to provide the osmotic pressures necessary to move dissolved iodine through the entire specimen. Pairing such concentrations with appropriate staining durations provides the opportunity for full penetration of the more voluminous anatomical regions of interest that are typical of post-embryonic vertebrates. Importantly, this rule of thumb appears to hold true only up to a point, beyond which over-staining can become an issue. This threshold appears to be around 10% w/v (I_2KI) (specifically, without refreshing the solution throughout the staining period). While not necessarily true universally (e.g. a *Scurius* stained in 25% I_2KI for 48 days; Jeffery et al. 2011), beyond this approximate level of concentration, extended staining durations can lead to loss of tissue differentiation due to excessively high levels of X-ray attenuation during μCT-scanning (Gignac & Kley, 2014) or soft-tissue shrinkage (Vickerton et al. 2013; Cox & Faulkes, 2014).

In general, it is considered appropriate to stain small invertebrates and vertebrate embryos relatively weakly and briefly and larger post-embryonic vertebrates more strongly and for longer durations. However, exposing soft tissues to double-digit iodine concentrations should be done with care as this may produce contrast-enhanced image stacks that are unusable for research, and possibly destruction of the specimen itself. Therefore, we recommend size matching your specimens to those already well imaged in the literature (see Tables 1 and S1) and following similar protocols to obtain comparable results (also see 'Specimen Preparation Tips and Tricks' in Fig. 6).

Specimen imaging

Specific scanning parameters will be dictated to some extent by the hardware and software features of the specific imaging system being used. Regardless, researchers have been successful using more than a dozen micro- and nano-CT systems, including those manufactured by General Electric (Fairfield, CT, USA), Nikon (Tokyo, Japan), Siemens AG (Berlin, Germany), Bruker (Billerica, MA, USA), TriFoil Imaging (Chatsworth, CA, USA), Yxlon International GmbH (Hamburg, Germany), and Carl Zeiss AG (Oberkochen, Germany).

DiceCT techniques also appear to be relatively insensitive to the X-ray target material; beryllium, copper, molybdenum, and tungsten, which are each used by the CT-scanner manufacturers listed above, all work well with iodine-enhanced specimens (see Table S1). Indeed, other target materials, such as diamond, may also work comparably well (C.P.O., pers. obs.). Similarly, we have not detected any specific effect of filter composition. Researchers have used aluminum, copper, and beryllium filters of variable thickness to constrain their X-rays when needed, and each has been compatible with diceCT imaging. Notably, some intrinsic factors of CT systems related to the X-ray detector specifically – such as size in pixels, dynamic range, recovery rate, bit depth, read-out, and scintillator – may differentiate similar classes of scanning systems more so than other hardware features. For a comprehensive review on scanner hardware and physics, see Stock (2009).

The factor of greatest concern for scanning iodine-stained specimens is that they have been rendered far denser than is typical of metazoan soft tissues through absorption of iodine. Beam energies (e.g. voltage and current) will

Specimen Preparation Tips and Tricks

- While frozen specimens or those in long-term alcohol storage can produce quality imaging results, we generally recommend using the freshest specimens possible.
- Mix your own Lugol's staining solutions from dry ingredients (I_2 and KI) to ensure that you are getting the desired concentrations.
- To facilitate elemental iodine entering the solution, first add potassium iodide to water. Then, use a mortar and pestle to pulverize elemental iodine before mixing it into solution as well.
- Skinning specimens can facilitate faster diffusion of stain, particularly for adult specimens.
- If using a sucrose prewash, heat the water to facilitate complete dissolving of sucrose. Then, cool the solution in a refrigerator or freezer before use to prevent tissue damage.
- Regularly agitate your specimens by hand or with an electric rocker while they are in iodine solutions to facilitate even staining.
- If your Lugol's staining solutions lighten from their original reddish-brown color—or if they become completely clear—replenish them as necessary.
- Upon removal of specimens from staining solutions, blot away excess fluids to prevent movement artifacts during scanning due to fluid accumulating at the bottom of the specimen or its container.
- Regularly agitate your specimens with an electric rocker while destaining to facilitate more rapid leaching or chemical neutraliztion.

Fig. 6 Specimen Preparation Tips and Tricks: a compilation of methodological shortcuts and timesaving measures from the authors' collective experience, designed to help facilitate successful preparation and staining of diceCT specimens.

typically need to be higher for contrast-enhanced specimens than non-stained ones. This is particularly true when considering larger, post-embryonic vertebrate specimens for which beam energies reported in the literature (see Table S1) have been generally comparable to those used for imaging vertebrate fossils surrounded by matrix (Ketcham & Carlson, 2001). With these factors in mind, setting CT/μCT parameters should be considered a balance between generating powerful X-rays that can penetrate dense, iodine-imbued tissues while also minimizing visual noise, such as that caused by excessive X-ray attenuation, within the final μCT image stack. Notably, such noise typically increases with increased X-ray energy, so additional steps should be taken to reduce visual noise when imaging particularly dense specimens (Neu & Genin, 2014).

As with our staining recommendations, we suggest targeting beam parameters using similar values to those that have been shown to be successful in the literature based on comparably sized and stained specimens. These details are available in Tables 1 and S1. Reducing image noise can be achieved by modifying additional software parameters that can be set on many modern imaging systems. Specifically, these include detector exposure timing, multi-frame averaging, and rotation step length. Controlling the exposure of X-rays passing through a specimen for a specific amount of time (e.g. 100, 200 or 333 ms) allows the researcher to capture more or fewer photons. Similar to the situation with a conventional camera, capturing more photons provides for a less noisy image. The optimal exposure timing will be a balance between the time required to fully scan the entire specimen and the time available to capture a sufficient number of X-rays for each frame during the scanning process. The technicians and engineers who run these scanners will likely have the most valuable input for exposure timing on a scanner-by-scanner basis.

In addition, many μCT systems can take multiple X-ray images of the same frame and average those images. Averaging the data collected from several acquisitions of the same image frame helps to smooth out variances due, for example, to natural shifts in the population of X-rays generated by the target metal as well as unchecked thermal expansion of the X-ray tube during prolonged scans. Each of these series of frames is taken after the specimen is rotated relative to the X-ray target and detector, and reducing the length of the rotation provides a denser sample of data for reconstruction. Thus, the rotation step, when modifiable, can also reduce grayscale variances that result from undersampling by providing more X-ray data for reconstruction algorithms. Different combinations of exposure timing, multi-frame averaging, and rotation step length may be optimal for different scanner configurations. As with extended exposure timing, capturing multiple acquisitions of the same X-ray image and sampling more densely during specimen rotation prolongs the time required to fully scan each specimen, which can be an important practical barrier for some researchers. Many studies, particularly of small (and, therefore, not exceptionally dense) specimens have not needed to modify these parameters (see Table S1). Those that have modified them, however, have tended to adjust multi-frame image averaging, specifically. These studies have sampled between two and 12 frames (Degenhardt et al. 2010; Tahara & Larson, 2013; Cox & Faulkes, 2014; Gignac & Kley, 2014; Kleinteich et al. 2014) with three and eight being the most common (see Table S1). It may be worthwhile to scan the same specimen under different sets of these conditions, particularly when using μCT systems that have a 'fast scan' option. These data would be helpful for identifying system-specific configurations that can maximize imaging potential for a given amount of beam time (also see 'Specimen Imaging Tips and Tricks' in Fig. 7).

Specimen Imaging Tips and Tricks

- Use sealable plastic bags and press out air to prevent specimens from drying out during a scan and for maintaining clean mounting equipment. Avoid vacuum sealing pliable specimens that can deform under pressure.
- Gently tap the specimen on a countertop in its mounting unit to allow it to "settle" before scanning to minimize movement during scan.
- Use a test tube or aliquot tube to submerge small specimens in fluid (e.g. formalin, or ethanol for specimens stained in ethanol-based solutions) duringscanning to prevent desiccation.
- Use a 3-D printer to make mounting units for a variety of specimen sizes and secure specimens within each unit using packaging material (e.g. foam, bubble wrap).
- If you have ready access to a medical or μCT scanner, running shorter, low-quality scans iteratively is useful for checking the progress of staining before investing more time and money into longer, high-quality scans.
- Although it takes longer, averaging multiples of the same X-ray frame during CT scanning can substantially reduce noise in the final image stack.
- Minute shifts in specimen position during scanning can often be corrected mathematically by the scanner's software tools, but larger shifts may require resecuring and rescanning the specimen.
- To facilitate easier segmentation of hard and soft tissues, scan specimens before staining with parameters optimized for bone. Bony and soft-tissue regions of interest can be merged later when they have been rendered from both sets of scan data.

Fig. 7 Specimen Imaging Tips and Tricks: a compilation of methodological shortcuts and timesaving measures from the authors' collective experience, designed to help facilitate successful CT scanning of diceCT specimens.

Destaining specimens and long-term storage

Iodine staining is not permanent. The staining components of iodine-based contrast agents can be removed by two methods, leaching and chemical destaining. Leaching utilizes clean ethanol, methanol, water or a fresh solution of storage agent to withdraw iodine from a specimen. A stained specimen is submerged in the leaching solution, which displaces dissolved iodine in the specimen due to an osmotic imbalance between the specimen and the surrounding fluid medium. This process is slow, often taking many weeks, and requires regular refreshing of the leaching solution when it becomes saturated with iodine (D.J.P., pers. obs.). Given enough time, first the superficial-most tissues will return to their original color; following this, deeper tissues also will be leached of iodine. Researchers should be aware that iodine binds particularly well to glandular tissues and those with extremely glycolytic metabolisms, such as the lenses of the vertebrate eye (P.M.G. & N.J.K., pers. obs.). Even with sufficient time and regularly refreshed leaching solutions, tissues such as these may never fully release their bound iodine. Therefore, an additional approach to chemically destain the staining component(s) of iodine-based contrast agents may be required.

Based on clock reactions (Shakhashiri, 1983), titration experiments (Trevorrow & Fashena, 1935), and clinical procedures (Kondo et al. 2001), sodium thiosulfate ($Na_2S_2O_3$) is well known for reversing the staining effects of iodine. In solution, sodium thiosulfate reacts with dissolved iodine, reducing it to iodide (Jeffery et al. 1989). Unlike aqueous triiodide, which is red-brown, iodide is transparent. The effect of sodium thiosulfate, therefore, is to chemically destain soft tissues by alteration of the iodine species they contain (Schmidbaur et al. 2015). Fully submerging a stained specimen into an aqueous solution of sodium thiosulfate will achieve this result. The specimens should be exposed to at least twice as many molecules of dissolved sodium thiosulfate ($2S_2O_3^{2-}$) as elemental iodine molecules (I_2) from the original stain solution to fully reverse the color change. Schmidbaur et al. (2015) notes, however, that high concentrations ($\geq$ 10% w/v) of sodium thiosulfate may alter the properties of fixed specimens, rendering them softer and less well contrasted than non-stained conspecifics. Therefore, we recommend using $<$ 10% w/v concentrations of sodium thiosulfate for destaining whenever possible. This approach may require multiple destaining baths for well-stained specimens. Nonetheless, the first effects of destaining will be apparent within minutes, even at low concentrations (1% w/v) of sodium thiosulfate.

The time required to completely destain a specimen varies from a few hours (Schmidbaur et al. 2015) to a couple of days (A.C.M., pers. obs.). Following destaining, specimens may be placed in a long-term chemical storage solution (e.g. 70% ethanol). However, some remaining stain may continue to leach from specimens for a week or more. Thus, although specimens will remain stable in their storage solutions, we recommend refreshing these solutions as needed following destaining. It is important to note that destaining does not restore a specimen to its original chemical state: colorless iodide remains in the specimen after destaining. Therefore, diceCT specimens that have been destained with sodium thiosulfate must be considered chemically altered. Notably, however, such techniques permit continued use of the specimen for gross dissection and further diceCT staining as well as other visualization methods. Therefore, diceCT can be considered a reversible and non-destructive 3-D imaging tool for documenting metazoan soft-tissue anatomy.

The combinations of specimen preparation, staining, and imaging parameters that have yielded effective results have varied extensively. This would seem to speak to the multifaceted approaches that can be taken to successfully image vertebrate soft tissues using iodine-based contrast media. The capacities of I_2KI, I_2E, and I_2M to differentially bind to metazoan soft tissues prepared under numerous chemical protocols, along with iodine's capacity for attenuating X-

rays, sets diceCT up as a remarkably versatile and robust tool for imaging the soft-tissue anatomy of a vast array of extant organisms.

Reporting standards

Specimen fixation and storage, tissue staining, and CT imaging parameters all impact the ultimate quality and utility of any diceCT dataset. In fact, choices made as early as in the acquisition of specimens may have downstream effects that either promote or degrade the potential differentiation of contrast-enhanced soft tissues. However, there have been no standardized protocols for reporting relevant methods (see Tables 1 and S1). Lack of standardization in turn has hampered comparison of results among datasets and repeatability of the methods underlying highly successful studies.

Consistent reporting of methods is essential to overcome this issue. To this end, we strongly recommend that researchers publish certain specific parameters, including novel modifications to established techniques and use of yet-to-be-deployed imaging hardware. This will standardize the reporting process and allow for the integration and synthesis of older studies with data on new specimens. We recognize that in certain cases important data may not be known, such as early specimen history (e.g. fixation and storage histories of older museum specimens); however, any efforts authors can make to fill in these gaps have the potential to be exceptionally useful to those who might seek to build upon their results.

Specimen history, fixation, and storage

Studies to date indicate strongly that the quality of X-ray CT imaging of iodine-stained soft tissues is affected significantly by how specimens have been preserved and maintained. Thus, including details about the histories of specimens examined in any diceCT study will be key to further refining this general technique and the specific methodologies that underlie it. If these aspects of the procedure are not standardized, any incremental improvements achieved via changes in the staining agent (e.g. I_2KI, I_2E, I_2M), concentration or approach to immersion may be difficult to identify. Specifically, we recommend that all known data regarding specimen acquisition be reported.

The following questions should be answered in the methodological or supplemental sections of a study: Were materials borrowed as fixed museum specimens, recently deceased, or obtained alive and then fixed? In the case of the latter, details about euthanasia (e.g. any chemicals potentially involved) and reference to relevant protocols should be provided. Were the specimens initially frozen prior to being fixed? In studies of isolated body parts, was the structure of interest dissected out and fixed on its own, or was the whole specimen fixed with the structure *in situ* but later dissected out for staining? What type of fixative (e.g. formalin, paraformaldehyde, Dent's fixative, Bouin's solution, glutaraldehyde) was used, at what concentration, and for how long were the specimens fixed? Were specimens subsequently transferred to a different fluid storage medium (e.g. ethanol, methanol) following initial fixation and prior to staining? If so, for how long? Any one of these factors can have significant effects on the quality of diceCT imaging. For instance, freezing not only has the potential to distort the gross morphology of soft tissues (largely through the formation of ice crystals within and between such tissues; R.M.H., pers. obs.), it also can reduce the effectiveness of iodine staining of myelinated nervous tissues (P.M.G. & N.J.K., pers. obs.). The latter effect is also commonly seen in specimens that have been stored in ethanol following fixation (Fig. 4A). In addition, ethanol seems to interact in some circumstances with iodine to cause excessive tissue shrinkage (Vickerton et al. 2013).

Finally, regarding the specimens themselves, their ages or developmental stages (if known) and absolute sizes should be detailed. Specimen age can represent critical information, particularly for embryos, wherein some tissue and organ systems are not fully developed. Specimen size is also a particularly important variable as it helps to guide staining protocols, insomuch as larger specimens necessitate greater exposure to iodine-based staining solutions (Gignac & Kley, 2014) and may require different pre-treatment protocols or approaches to immersion.

Specimen preparation and iodine staining

The focus of specimen staining is primarily on maximizing the uptake of various species of iodine ions (Cooper, 2007) for any chosen concentration(s) of staining solution (e.g. I_2KI, I_2E, I_2M). With respect to specimen preparation and staining, the following questions should be answered: Were any physical or chemical alterations made to specimens between storage and scanning, or were any techniques used for enhancing iodine mobilization? Physical modifications, including skinning, decapitation, removal of body parts, or trepanation, should be described in detail. Each of these techniques exposes internal surfaces, which enhances iodine diffusion into deeper soft tissues. Were any additional specimen treatments beyond fixation and storage carried out (e.g. sucrose baths, embedding, hydrogel stabilization; Lee & Timasheff, 1981; Degenhardt et al. 2010; Mizutani & Suzuki, 2012; Wong et al. 2013)? Such procedures may introduce additional chemicals with varying affinities for iodine and, thus, may impact visual interpretations. Finally, were specimens agitated while staining as a means to accelerate the staining process? Depending on the technique used, agitation could be continuous or periodic (i.e. at regular intervals). For example, smaller specimens allow for using an electronic rocker continuously whereas larger ones may require periodic manual agitation.

Regardless, the nature and frequency of agitation episodes should be reported.

There is an additional important technical consideration when using Lugol's iodine in particular. Whether the solution was mixed from solid components (i.e. crystalline iodine and granular potassium iodide) or was a pre-made volume of Lugol's iodine purchased as a stock solution may affect staining. For custom-mixed solutions, the source of the water should be indicated (e.g. deionized water, tap water, reverse osmosis water). The staining potency of Lugol's iodine can diminish over time with exposure to strong light sources (e.g. sunlight) due to the volatility of triiodide/iodide redox reactions (Jeffery et al. 1989), to which pre-prepared solutions are acutely vulnerable. (Note: storage in blacked-out or amber glass containers will mitigate this issue.) During the staining process, concentrations of Lugol's iodine and staining durations are obviously critical, and should be reported consistently along with the number and frequency of solution changes (e.g. daily, weekly). In particular, some authors choose to report concentrations of Lugol's solution in terms of I_2 only, expressing such concentrations as weight of I_2 per volume of solution (I_2, w/v). Others, however, report total solute concentrations [i.e. weight of I_2KI per volume of solution (I_2KI, w/v); see Gignac & Kley, 2014]. This distinction is critical because misinterpretations by other workers could lead to their adopted use of erroneously weak or strong solutions, which can either understain specimens or permanently deform them due to extreme shrinkage, respectively (Pauwels et al. 2013; Vickerton et al. 2013; Buytaert et al. 2014). We recommend reporting total solute concentrations of I_2KI (w/v) because the iodine that contributes to staining comes from both I_2 and KI (Degenhardt et al. 2010). (Note: practitioners should be aware that some retailers advertise pre-made Lugol's iodine solutions in concentrations of I_2 only, so reporting both total solute and elemental iodine concentrations may be appropriate in some situations.)

CT imaging and data reconstruction

Settings for CT and μCT parameters have varied substantially across contrast-enhanced imaging studies. To facilitate the ability of researchers to replicate CT scanner conditions as closely as is practicable, we recommend that all studies report a specific set of variables related to X-ray image capture and data reconstruction. Specifically, it is of vital importance for diceCT researchers to report the make and model of the scanner(s) that they use, as well as relevant scanner settings.

Some scanner systems are more appropriate for imaging certain types of specimens than others (e.g. due to specimen size, degree of mineralization, density of contrast agent within the specimen). For studies seeking to quantify values of grayness in particular, an important consideration is whether the scanning system generates a parallel or cone-shaped beam. Whereas Hounsfield units (HUs) are reported for images generated by parallel-beam scanners, they are not necessarily appropriate for those generated by scanners using cone-shaped beams, whose average X-ray density decreases substantially as a function of distance from the source. In the latter case, grayscale values (GVs) are most appropriate to report unless a conversion factor from GVs to HUs has been determined experimentally (i.e. using phantoms) both for the specific configuration of the μCT scanner and for the location of the imaged specimen(s) within the scan volume of that specific system (see Mah et al. 2010; Valiyaparambil et al. 2012; Tahara & Larson, 2013; Razi et al. 2014).

The scanner settings used in generating the X-ray beam will also affect scan results. When preparing the scan, users typically adjust energy variables that contribute to beam generation, specifically, peak kilovoltage (kVp; often reported as kV) and current (μA). The X-ray beam is generated from a metal 'target' such as tungsten or molybdenum, and the range of X-ray wavelengths generated at a given combination of kVp and μA differs slightly based on the composition of the target. These parameters are among the most important for effectively imaging contrast-enhanced specimens, and are, therefore, among the most important to report. In addition, a complete methods section should describe the filter used, if any. CT scanner X-ray beams are often passed through a filter (e.g. varying thicknesses of aluminum, copper, glass, tin) to prevent imaging artifacts such as beam hardening by constraining the X-ray wavelengths that reach specimens. Thus, the composition and thickness of any filters are additional important details bearing on imaging reproducibility.

Image capture by the scanning system also can be manipulated by altering scanner calibrations, exposure timing, or image averaging. A thorough methods section should answer the following questions concerning calibrations: Were any scanner calibrations made? These may include adjustments to the gain (referred to as sensitivity by some manufacturers) as well as geometric corrections that can reduce image noise. These should be described. Additionally, was the X-ray detector activated for specifically controlled periods of time (e.g. 100, 200, 333 ms)? It also should be clear whether the CT system was set to average multiple acquisitions of the same frame. Long exposures paired with multifold image averaging can generate exceptionally clear contrast-enhanced images, but this benefit comes at the expense of greatly increased scan times (see also 'Case studies and recommendations' section above).

Finally, voxel size, bit depth, and post-processing of image data are also important parameters to report in order to ensure that final image quality is reproducible and comparable among studies. For example, the voxel size (including inter-slice spacing for anisometric voxels) and bit depth that were sampled should be stated clearly; the total range of HUs or GVs (referred to collectively as 'gray values'

here) that can be represented in scan data is determined by bit depth. The same specimens will appear different in 8-bit vs. 16-bit images due to the different ranges of gray values that can be represented (i.e. 265 vs. 65 536 in 8-bit vs. 16-bit images, respectively). Greater bit depths (i.e. $\geq$ 16-bit images) are likely to become increasingly important for visualizing subtle differences between the boundaries of adjacent structures in contrast-enhanced CT.

Post-processing steps also should be detailed. Algorithmic modifications of the scan data to remove, for example, ring artifacts associated with beam hardening should be reported, as these modify gray values within the entirety of the image stack to subtract the blemish. Each such post-processing step, therefore, can subtly or greatly alter the differentiability of various soft-tissue structures in diceCT image sets. Adjustments to contrast made in photo editing software for print publication should be reported as well.

Authors might also consider publishing additional useful parameters such as overall scan time, image file type (e.g. TIFF, DICOM), and number of slices. These details can be useful to those planning for facilities usage or data storage and analysis of diceCT imaging for the first time. To facilitate the reporting of essential parameters, we have developed a sample reporting spreadsheet (Supporting Information Table S2), which is designed to fit within most standard laboratory notebooks. This document, or a modified version, is intended to be of help in ensuring the full gathering of specimen storage, preparation, and CT parameters during each stage of diceCT imaging research.

Other contrast agents

In addition to iodine, several metallic contrast agents have been used successfully to enhance soft-tissue contrast in X-ray images (see Metscher, 2009a,b; Mizutani & Suzuki, 2012; Pauwels et al. 2013; Descamps et al. 2014). Although it is beyond the scope of this overview to detail these potential alternatives to iodine, we think it prudent to ensure that researchers are aware of such other contrast agents. Additional visualization agents include diffusible stains, similar to iodine-based I_2KI, I_2E, and I_2M, as well as radiopaque perfusion compounds that are injected directly into the anatomical regions of interest for visualizing lumina, such as those within blood vessels. Commonly used examples of diffusion and perfusion-based agents include molybdenum [as phosphomolybdic acid (PMA)], tungsten [as phosphotungstic acid (PTA)], mercury [as mercuric chloride ($HgCl_2$)], osmium [as osmium tetroxide (OsO_4)], barium (as an additive to injectable latex), and silver [as silver proteinate (SP) and silver nitrate (e.g. Golgi's stain)], among others. Examples of contrast-enhanced images using some of these alternative contrast agents are illustrated alongside iodine-based and histological images in Fig. 8. Each compound has its own benefits (and thus may be more effective for certain research goals), including its capacity to stain cartilage, rate of diffusion, tissue specificity, and restriction to specific anatomical compartments of interest. At the same time, some of these metallic compounds are difficult to work with due to high toxicity and/or costs, state and federal restrictions on distribution and usage (i.e. in the USA, distribution of iodine $>$ 2% purity is regulated by the Drug Enforcement Agency), and special storage and/or disposal requirements.

Many researchers have used these alternatives successfully and given thorough reports of the details of their successes throughout the literature. We have synthesized these details along with our own experiences into Supporting Information Table S3, which provides a summary of diffusion- and perfusion-based approaches. This table includes recommendations for targeting specific tissue types, specimen preparation techniques, staining durations, equipment needed, and availability through commercial vendors as well as storage, stability, and disposal requirements, among other details. Each category is broken down by contrast agent. These agents are listed alongside various forms of iodine-based stains (I_2KI, I_2E, I_2M) as well, so that researchers who are unsure about which contrast agent best fits their needs, can easily identify the various attributes of each.

The future of diceCT

The iodine staining that makes diceCT possible is minimally destructive and potentially reversible (e.g. using an aqueous solution of sodium thiosulfate; Schmidbaur et al. 2015; see also 'Destaining specimens and long-term storage' above). This affords investigators the opportunity to supplement their 3-D imaging data with histological staining and sectioning, vascular injections, or other research and visualization techniques for the same specimen. DiceCT techniques differentiate soft tissues with high degrees of precision that can enhance or even exceed what can be discerned through gross dissection or non-enhanced CT scanning. Issues of fundamental anatomical importance, such as the precise relationships between soft tissues and bony elements, or the interrelationships between different soft tissues themselves, are clarified by the careful application of contrast-enhancing agents.

Beyond the benefits diceCT offers to descriptive anatomists, this approach also allows for the quantification of soft-tissue morphology, including linear dimensions and volumetric data. Three-dimensional rendering of diceCT images facilitates precise measurement of important functional anatomical parameters such as muscle volumes (Holliday et al. 2013; Lautenschlager et al. 2013), muscle orientations (Hautier et al. 2012), fascicle lengths (Jeffery et al. 2011; Vickerton et al. 2014), physiological cross-sectional areas (Cox et al. 2011, 2012; Vickerton et al. 2014) and, potentially, physiological differences both between and within muscles (e.g. oxidative vs. glycolytic fibers; Gignac & Kley, 2014). Similarly, diceCT can facilitate neurological

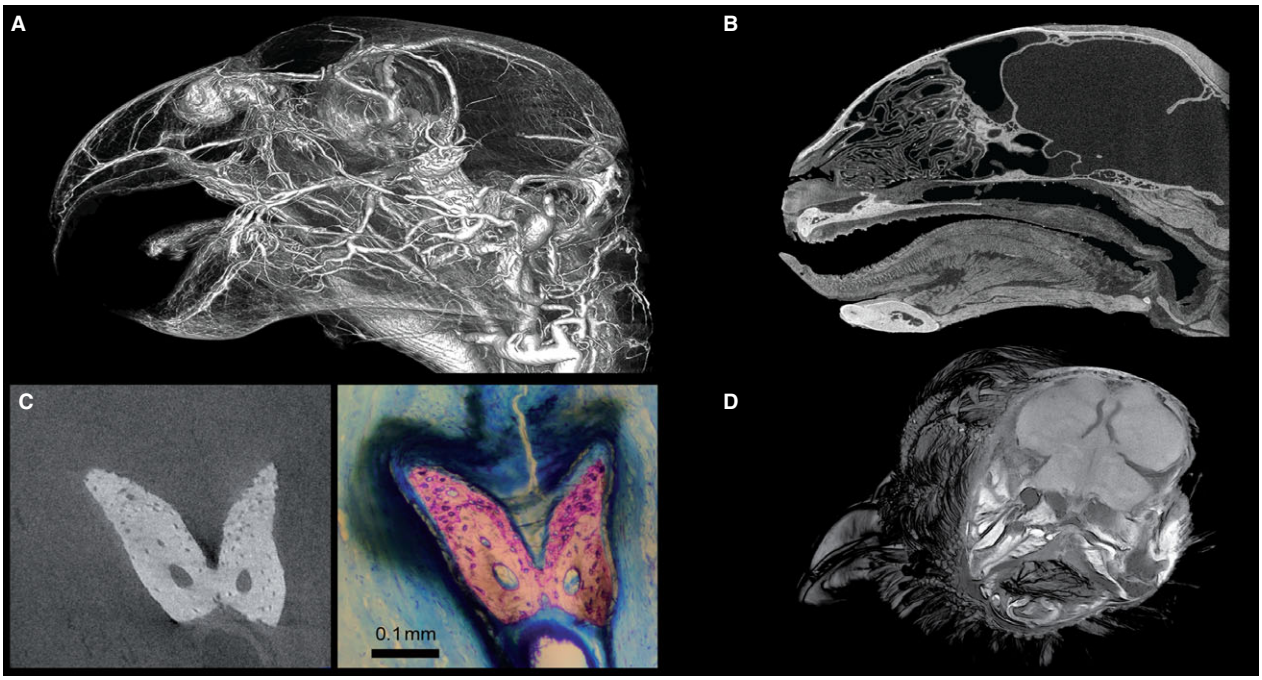

Fig. 8 Alternative perfusion-based (A) and diffusion-based (B, C [right], D) methods for enhancing soft-tissue visualizations compared with diceCT imaging techniques (C [left], D). (A) A 3-D volume rendering of the cranial vasculature of an African gray parrot (*Psittacus erithacus*; anterior is left) that was perfused with BriteVu™. (B) Sagittal slice through the head of a domestic cat (*Felis catus*; anterior is left) stained with phosphomolybdic acid (PMA), demonstrating nasal and laryngeal cartilages and lingual musculature. (C) DiceCT image (left) of the baculum of a common pipistrelle bat (*Pipistrellus pipistrellus*) compared with a histological section (right) of the same specimen (anterior is top; modified from Herdina et al. 2015a, b). (D) Posterolateral view of a 3-D volume rendering of the anterior portion of the head of a common pheasant (*Phasianus colchicus*; anterior toward the left) prepared using diceCT imaging (diffusible) for comparison to (A) and (B). Vasculature is particularly well visualized using injection techniques (A), whereas other tissues and spaces within the body cannot be readily imaged using this technique. Phosphomolybdic acid (B) stains muscle and hyaline cartilage, allowing for clear resolution of fiber attachment locations; while it also stains neural tissue, poor penetration through the cranium leaves the brain unstained. Histological preparations (C) are capable of targeting tissues with great specificity but are time-consuming and difficult to translate into 3-D. Further documentation for a wide range of alternative contrast agents, including the categories of histological tissues that can be readily visualized for each, can be found in Table S3. Preparation, staining, and scanning parameters for diceCT specimens (C, D) can be found in Tables 1 and S1. Specimen images contributed by A.N.H., C.P.O., J.A.C., M.S.E., and Z.L.

studies of the central and peripheral nervous systems and measurement of structures within the brain itself, offering the capability to quantify size, shape, volume, and linear dimensions of neuroanatomical structures and their interconnections (Metscher, 2013; Gignac & Kley, 2014). In fact, the same specimens once stained with Lugol's iodine may be used subsequently in histological studies to verify and validate these findings (Jeffery et al. 2011; Herdina et al. 2015b). In essence, each specimen may reveal its own morphology recursively through the implementation of multiple imaging modalities, thereby providing a remarkable amount of information from only a single specimen.

The datasets from diceCT studies are accessible via a wide range of imaging and analysis software, and the ability to share these digital datasets widely and rapidly is of great use to the biological sciences community. Combining important anatomical information into 'cybertypes' (Godfray, 2007; Faulwetter et al. 2013) that house digital image datasets on the hard- and soft-tissue morphologies of particular taxa would be highly valuable to a great many researchers. Interconnecting these data with genetic sequences and ecological information could be a dynamic and invaluable means by which to stitch together important, but often disparate, sources of biological information. For example, high-performance-running mouse strains are known to possess different muscle phenotypes (Houle-Leroy et al. 2003; Syme et al. 2005; Hannon et al. 2008), which have fiber orientations, fascicle lengths, physiological cross-sectional areas, and physiologies that could be visualized and documented in 3-D, using diceCT methods. These data could not only contribute to morphological databases such as DigiMorph (www.digimorph.org), but also the Mouse Phenome Database (Houle-Leroy et al. 2003; Guderley et al. 2006; Ring et al. 2015).

Accurate muscle reconstruction and modeling is critical to paleontological and biomechanical investigations of complex anatomical systems such as the vertebrate feeding apparatus. Computational methods, including finite element analysis, lever mechanics, inverse kinematics, and 3-D functional anatomical models all require input from muscle

morphology and physiology, but in varied formats depending on the software. DiceCT will help validate muscle sizes, angles of pennation, and physiological estimates, thereby increasing inferential and computation rigor and accuracy across similar investigations. Such cybertypes could link elements of multiple online repositories and even incorporate population subsamples, complete with phenotypic 'averages' and quantified ranges of variance for a species, including how variables of interest might change across development (Wong et al. 2012). Regardless of the precise nature of such data sharing, diceCT is poised to play an important role in the future of documenting anatomical diversity, providing transformative new insights into the developmental, functional, ecological, and evolutionary relationships of both vertebrate and invertebrate taxa.

The importance of biomechanical and kinematic models in the field of biology is well known. However, it can be complicated to study the morphological and physiological underpinnings of behavior *in vivo*. Modeling the function and performance of, for example, musculoskeletal levers used in locomotion or heat-transferring structures like vascular retia, can be a time-intensive task that requires IACUC and/or IRB approvals to conduct live-animal studies. The use of contrast agents like Lugol's iodine can supplement such studies by increasing sample sizes, documenting the delicate anatomy of particularly small species that might not be amenable to experimentation, or even standing in for, if not truly replacing, live animal studies as Tsai & Holliday (2015) suggest. Indeed, a small overall number of specimens can provide insights into a far wider range of functional anatomical questions because of the nearly holistic nature of diceCT data collection (Tsai & Holliday, 2011; George & Holliday, 2013; Holliday et al. 2013). At the same time, these same research specimens can be used to develop 3-D anatomical atlases (see Holliday et al. 2013) for educationally focused needs, thereby doubling the potential value of diceCT specimens for roles both in the laboratories and classrooms of anatomy and physiology, gross human anatomy, comparative vertebrate anatomy, and generalized organismal biology courses throughout secondary, post-secondary, graduate, and medical school curricula (Spaw & Witmer, 2013, 2014).

Today, the diceCT community is small but growing. There are still major scientific hurdles to overcome before iodine-based contrast enhancement can be considered a mature research tool. Unresolved issues primarily concern the largely undocumented effects of specimen size, preparation, extent of iodine staining, and μCT system parameters. It is imperative that the effects of these variables are identified and their impacts on contrast-enhanced imaging quality become better understood. At present, every imaging success and many imaging failures represent important data points towards the broader understanding of organism- and tissue-specific interactions with iodine. Similarly, there may be currently unidentified hardware and software optimizations for improving the quality of diceCT image stacks that those among the research community have yet to discover. Growing this community will make it more likely that we will each benefit from the important discoveries made in just a single CT lab. Standard protocols for destaining iodine-imbued specimens have the potential to augment access to research collections through the promise of generating holistic, valuable, and otherwise inaccessible data while returning such specimens to their home collections, unmolested. As we move forward, it may be possible and prudent to develop specimen preparation and imaging protocols that are specific to the academic aims and stewardship requirements of natural history collections.

Here we aim to facilitate the adoption of diceCT as part of a standard toolkit in the field of animal morphology. For methods to continue improving, the protocols for generating diceCT images must be further streamlined and more data provided on the techniques employed. Standardization in the reporting of methods is key to identifying areas for improvement. At the same time, the growing diceCT community must look to overcome the challenges of large specimen size, better assess variables correlated with tissue deformation or shrinkage, and improve protocols for the targeted contrast enhancement of specific tissues (e.g. the potential efficacy of iodine perfusion methodologies). Experiences outlined here by 'veteran' practitioners should enable the community to grow more rapidly by helping researchers avoid the hurdles that could otherwise stymy the broader adoption of this potentially transformative 3-D imaging tool, or lead to ineffectual or problematic staining effects. A new digital web portal (www.diceCT.com) is intended as a hub for the diceCT community. This portal provides web pointers to the newest studies that employ diceCT techniques and a forum for ongoing conversations about methodological optimizations, novel staining protocols, and new hardware. Through this initiative, we anticipate robust growth within the diceCT community and the realization of new horizons in contrast-enhanced imaging that are only now just beginning to emerge.

Acknowledgements

We thank The University of Texas (UT) at Austin, the Jackson School of Geosciences, and the UTCT Laboratory for providing facilities support and sponsorship for the working group meeting that led to this publication. B. D. Metscher participated in the Austin Working Group Meeting, which served as the basis for this manuscript, and provided exceptionally helpful insights during its development. M. Hill, H. D. O'Brien, H. Tobbin, and N. Westphal provided conceptual and technical support. A. M. Balanoff, M. E. Gold, A. Khan, D. W. Krause, M. A. Norell, R. Ridgely, A. H. Turner, A. Watanabe, E. Westwig, S. Werning, and F. Zachos aided in facilities and specimen access. We also thank the reviewers of an earlier version of this manuscript for the insights and constructive criticisms they provided. C.P.O. was supported by

A. Bhullar and NIH T32 HD009007. This work was supported financially by the National Science Foundation (NSF IOS-0749750 and NSF EAGER 1450842 awarded to N.J.K.; NSF DEB-1457180 and NSF EAGER 1450850 awarded to P.M.G.) as well as the Stony Brook University Department of Anatomical Sciences (N.J.K. and P.M.G.) and the Oklahoma State University Center for Health Sciences Department of Anatomy and Cell Biology (P.M.G.). BriteVu™ is a metallic perfusion product developed and sold by Scarlet Imaging, LLC, of which co-author M.S.E is the founder and president.

Author contributions

Conceived project: P.M.G., N.J.K., J.A.C., M.W.C., ACM; collected data: P.M.G., N.J.K., J.A.C., M.W.C., A.C.M., D.C., I.C., P.G.C., J.D.D., C.M.E., M.S.E., R.M.H., A.N.H., C.M.H., Z.L., K.M., S.M., J.M., C.P.O., D.J.P., M.L.T., H.P.T., L.M.W.; analyzed and interpreted data: P.M.G., N.J.K., J.A.C., M.W.C., A.C.M., D.C., I.C., P.G.C., J.D.D., C.M.E., M.S.E., R.M.H., A.N.H., C.M.H., Z.L., K.M., S.M., J.M., C.P.O., D.J.P., M.L.T., H.P.T., L.W.M.; wrote paper: P.M.G., N.J.K., J.A.C., M.W.C., A.C.M., D.C., I.C., P.G.C., J.D.D., C.M.E., M.S.E., R.M.H., A.N.H., C.M.H., Z.L., K.M., S.M., J.M., C.P.O., D.J.P., M.L.T., H.P.T., L.W.M.; created figures: P.M.G., N.J.K., J.A.C., A.C.M., C.M.E., M.S.E., R.M.H., A.N.H., C.M.H., Z.L., K.M., J.M., C.P.O., H.P.T., L.M.W.

References

Akkari N, Enghoff H, Metscher BD (2015) A new dimension in documenting new species: high-detail imaging for myriapod taxonomy and first 3D cybertype of a new millipede species (Diplopoda, Julida, Julidae). *PLoS ONE* **10**, e0135243.

Aslanidi OV, Nikolaidou T, Zhao J, et al. (2013) Application of micro-computed tomography with iodine staining to cardiac imaging, segmentation, and computation model development. *IEEE Trans Med Imaging* **32**, 8–17.

Balanoff AM, Bever GS, Colbert MW et al. (2015) Best practices for digitally constructing endocranial casts: examples from birds and their dinosaurian relatives. *J Anat* doi: 10.1111/joa.12378.

Baverstock H, Jeffery NS, Cobb SN (2013) The morphology of the mouse masticatory musculature. *J Anat* **223**, 46–60.

Buytaert J, De Greef D, Aerts P, et al. (2014) Volume shrinkage of bone, brain and muscle tissue in sample preparation for micro-CT and light sheet florescence microscopy (LSFM). *Microsc Microanal* **20**, 1208–1217.

Cooper RA (2007) Iodine revisited. *Intl Wound J* **4**, 124–137.

Cox PG, Faulkes CG (2014) Digital dissection of the masticatory muscles of the naked mole-rat, *Heterocephalus glaber* (Mammalia, Rodentia). *PeerJ* **2**, e448.

Cox PG, Jeffery N (2011) Reviewing the morphology of the jaw-closing musculature in squirrels, rats, and guinea pigs with contrast-enhanced micro-CT. *Anat Rec* **294**, 915–928.

Cox PG, Fagan MJ, Rayfield EJ, et al. (2011) Finite element modeling of squirrel, guinea pig and rat skulls: using geometric morphometrics to assess sensitivity. *J Anat* **219**, 696–709.

Cox PG, Rayfield EJ, Fagan MJ, et al. (2012) Functional evolution of the feeding system in rodents. *PLoS ONE* **7**, e36299.

de Crespigny A, Bou-Reslan H, Nishimura MC, et al. (2008) 3D micro-CT imaging of the postmortem brain. *J Neurosci Methods* **171**, 207–213.

Degenhardt K, Wright AC, Horng D, et al. (2010) Rapid 3-D phenotyping of cardiovascular development in mouse embryos by micro-CT with iodine staining. *Circ Cardiovasc Imaging* **3**, 314–322.

Descamps E, Sochacka A, Kegel BD, et al. (2014) Soft tissue discrimination with contrast agents using micro-CT scanning. *Belg J Zool* **144**, 20–40.

Dougherty LR, Rahman IA, Burdfield-Steel ER, et al. (2015) Experimental reduction of intromittent organ length reduces male reproductive success in a bug. *Proc R Soc B* **282**, 20150724.

Düring DN, Ziegler A, Thompson CK, et al. (2013) The songbird syrinx morphome: a three-dimensional, high-resolution, interactive morphological map of the zebra finch vocal organ. *BMC Biol* **11**, 1.

Faulwetter S, Vasileiadou A, Kouratoras M, et al. (2013) Micro-computed tomography: introducing new dimensions to taxonomy. *ZooKeys* **263**, 1–45.

Fernández R, Kvist S, Lenihan J, et al. (2014) Sine systemate chaos? A versatile tool for earthworm taxonomy: non-destructive imaging of freshly fixed and museum specimens using micro-computed tomography. *PLoS ONE* **9**, e96617.

George ID, Holliday CM (2013) Trigeminal nerve morphology in *Alligator mississippiensis* and its significance for crocodyliform facial sensation and evolution. *Anat Rec* **296**, 670–680.

Gignac PM, Kley NJ (2014) Iodine-enhanced micro-CT imaging: methodological refinements for the study of soft-tissue anatomy of post-embryonic vertebrates. *J Exp Zool B Mol Dev Evol* **322B**, 166–176.

Godfray HCJ (2007) Linnaeus in the information age. *Nature* **446**, 259–260.

Guderley H, Houle-Leroy P, Diffee GM, et al. (2006) Morphometry, ultrastructure, myosin isoforms, and metabolic capacities of the 'mini muscles' favoured by selection for high activity in house mice. *Comp Biochem Physiol B* **144**, 271–282.

Hannon RM, Kelly SA, Middleton KM, et al. (2008) Phenotypic effects of the "mini-muscle" allele in a large HR x C57BL/6J mouse backcross. *J Hered* **99**, 349–354.

Harris LD, Robb RA, Yuen TS, et al. (1979) Display and visualization of three-dimensional reconstructed anatomic morphology: experience with the thorax heart, and coronary vasculature of dogs. *J Comput Assist Tomogr* **3**, 439–446.

Hautier L, Lebrun R, Cox PG (2012) Patterns of covariation in the masticatory apparatus of hystricognathous rodents: implications for evolution and diversification. *J Morphol* **273**, 1319–1337.

Herdina AN, Herzig-Straschil B, Hilgers H, et al. (2010) Histomorphology of the penis bone (baculum) in the gray long-eared bat *Pleocotus austriacus* (Chiroptera, Vespertilionidae). *Anat Rec* **293**, 1248–1258.

Herdina AN, Kelly DA, Jahelkova H, et al. (2015a) Testing hypotheses of bat baculum function with 3-D models derived from micro-CT. *J Anat* **226**, 229–235.

Herdina AN, Plenk H Jr, Benda P, et al. (2015b) Correlative 3D-imaging of *Pipistrellus* penis micromorphology: validating quantitative microCT images with undecalcified serial ground section histomorphology. *J Morphol* **276**, 695–706.

Holliday CM, Tsai HP, Skiljan RJ, et al. (2013) A 3-D interactive model and atlas of the jaw musculature of *Alligator mississippiensis*. *PLoS ONE* **8**, e62806.

Hopkins TM, Heilman AM, Liggett JA, et al. (2015) Combining micro-computed tomography with histology to analyze biomedical implants for peripheral nerve repair. *J Neurosci Methods* **255**, 122–130.

Houle-Leroy P, Guderley H, Swallow JG, et al. (2003) Artificial selection for high activity favors mighty mini-muscles in house mice. *Am J Physiol Regul Integr Comp Physiol* **284**, R433–R443.

Humason GL (1972) *Animal Tissue Techniques*. 3rd edn. San Francisco: W. H. Freeman and Company.

Hutchinson JC, Arthurs OJ, Ashworth MT et al. (2016) Clinical utility of postmortem micro-computed tomography of the fetal heart: diagnostic imaging versus macroscopic dissection. *Ultrasound Obstet Gynecol* **47**, 58–64.

Jaspers C, Carstensen J (2009) Effect of acid Lugol solution as preservative on two representative chitineous and gelatinous zooplankton groups. *Limnol Oceanogr Methods* **7**, 430–435.

Jeffery GH, Bassett J, Mendham J, et al. (1989) *Vogel's Textbook of Quantitative Chemical Analysis*. 5th edn. New York: Wiley & Sons, Inc.

Jeffery NS, Stephenson RS, Gallagher JA, et al. (2011) Micro-computed tomography with iodine staining resolves the arrangement of muscle fibres. *J Biomech* **44**, 189–192.

Ketcham RA, Carlson WD (2001) Acquisition, optimization and interpretation of X-ray computed tomographic imagery: applications to the geosciences. *Comput Geosci* **27**, 381–400.

Kleinteich T, Gorb SN (2015a) The diversity of sticky frog tongues. *Bruker microCT User Mtg Abstracts,* **2015–18**, 1–4.

Kleinteich T, Gorb SN (2015b) Frog tongue acts as muscle-powered adhesive tape. *R Soc Open Sci* **2**, 150333.

Kleinteich T, Conway KW, Gorb SN, et al. (2014) What's inside a fishy suction cup? *Bruker microCT User Mtg Abstracts,* **2014–14**, 1–4.

Kondo H, Fukuda H, Ono H, et al. (2001) Sodium thiosulfate solution spray for relief of irritation caused by Lugol's stain in chromoendoscopy. *Gastrointest Endosc* **53**, 199–202.

Lautenschlager S, Bright JA, Rayfield EJ (2013) Digital dissection – using contrast-enhanced computed tomography scanning to elucidate hard- and soft-tissue anatomy of the Common Buzzard *Buteo buteo*. *J Anat* **224**, 412–431.

Lee JC, Timasheff SN (1981) The stabilization of proteins by sucrose. *J Biol Chem* **256**, 7193–7201.

Lenihan J, Kvist S, Fernández R, et al. (2014) A dataset comprising four micro-computed tomography scans of freshly fixed and museum earthworm specimens. *Gigascience* **3**, 6.

Li Z, Clarke JA (in press) The craniolingual morphology of waterfowl (Aves, Anseriformes) and its relationship with feeding mode revealed through contrast-enhanced X-ray computed tomography and 2-D morphometrics. *J Evol Biol*.

Mah P, Reeves TE, McDavid WD (2010) Deriving Hounsfield Units using grey levels in cone beam computed tomography. *Dentomaxillofac Radiol* **39**, 323–335.

Metscher BD (2009a) Micro-CT for comparative morphology: simple staining methods allow high-contrast 3D imaging of diverse non-mineralized animal tissues. *BMC Physiol* **9**, 11.

Metscher BD (2009b) Micro-CT for developmental biology: a versatile tool for high-contrast 3-D imaging at histological resolutions. *Dev Dyn* **238**, 632–640.

Metscher BD (2013) Biological applications of X-ray microtomography: imaging micro-anatomy, molecular expression and organismal diversity. *Microsc Anal (Am Ed)* **27**, 13–16.

Mizutani R, Suzuki Y (2012) X-ray microtomography in biology. *Micron* **43**, 104–115.

Neu CP, Genin GM (2014) *Handbook of Imaging in Biological Mechanics*. Boca Raton: CRC Press.

Pauwels E, Van Loo E, Cornillie P, et al. (2013) An exploratory study of contrast agents for soft tissue visualization by means of high resolution X-ray computed tomography imaging. *J Microsc* **250**, 21–31.

Razi T, Niknami M, Ghazani FA (2014) Relationship between Hounsfield Unit in CT scan and grayscale in CBCT. *J Dent Res Dent Clin Dent Prospects* **8**, 107–110.

Ring N, Meehan TF, Blake A et al. (2015) A mouse informatics platform for phenotypic and translational discovery. *Mamm Genome* **26**, 413–421.

Schmidbaur H, Keklikoglou K, Metscher BD, et al. (2015) Exploring methods to remove iodine and phosphotungstic acid stains from zoological specimens. *Bruker microCT User Mtg Abstracts,* **2015–21**, 1–8.

Shakhashiri B (1983) *Chemical Demonstrations: A Handbook for Teachers of Chemistry*, Vol. **3**. Madison: University of Wisconsin Press.

Silva JMS, Zanette I, Noël PB, et al. (2015) Three-dimensional non-destructive soft-tissue visualization with X-ray staining micro-tomography. *Sci Rep* **5**, 14088.

Sombke A, Lipke E, Michalik P et al. (2015) Potential and limitations of X-ray micro-computed tomography in arthropod neuroanatomy: a methodological and comparative survey. *J Comp Neurol* **523**, 1281–1295.

Spaw A, Witmer LM (2013) Novel anatomical analysis of human embryos using iodine staining and micro-computed tomography (CT scanning). *FASEB J* **27**, 531.4.

Spaw A, Witmer LM (2014) Fetal developmental anatomy of the human cardiovascular and central nervous systems using Lugol's iodine staining and micro-computed tomography. *FASEB J* **28**, 923.6.

Stephenson RS, Boyett MR, Hart G, et al. (2012) Contrast enhanced micro-computed tomography resolves the 3-dimensional morphology of the cardiac conduction system in mammalian hearts. *PLoS ONE* **7**, e35299.

Stock SR (2009) *MicroComputed Tomography: Methodology and Applications*. Boca Raton: CRC Press.

Syme DA, Evashuk K, Grintuch B, et al. (2005) Contractile abilities of normal and 'mini' triceps surae muscles from mice (*Mus domesticus*) selectively bred for high voluntary wheel running. *J Appl Physiol* **99**, 1308–1316.

Tahara R, Larson HCE (2013) Quantitative analysis of microscopic X-ray computed tomography imaging: Japanese quail embryonic soft tissue with iodine staining. *J Anat* **223**, 297–310.

Tobita K, Liu X, Lo CW (2010) Imaging modalities to assess structural birth defects in mutant mouse models. *Birth Defects Res C Embryo Today* **90**, 176–184.

Trevorrow V, Fashena G (1935) The determination of iodine in biological material. *J Biol Chem* **110**, 29–38.

Tsai HP, Holliday CM (2011) Ontogeny of the alligator cartilago transiliens and its significance for sauropsid jaw muscle evolution. *PLoS ONE* **6**, e24935.

Tsai HP, Holliday CM (2015) Articular soft tissue anatomy of the archosaur hip joint: structural homology and functional implications. *J Morphol* **276**, 601–630.

Valiyaparambil JV, Yamany I, Ortiz D, et al. (2012) Bone quality evaluation: comparison of cone beam computed tomography

and subjective surgical assessment. *Int J Oral Maxillofac Implants* **27**, 1271–1277.

Vickerton P, Jarvis J, Jeffery NS (2013) Concentration-dependent specimen shrinkage in iodine-enhanced microCT. *J Anat* **223**, 185–193.

Vickerton P, Jarvis J, Gallagher JA, et al. (2014) Morphological and histological adaptation of muscle and bone to loading induced by repetitive activation of muscle. *Proc R Soc Lond B Biol Sci* **281**, 20140786.

Wallingford VH (1953) The development of organic iodine compounds as X-ray contrast media. *J Am Pharm Assoc* **42**, 721–728.

Webb WR, Brant W, Major N (2005) *Fundamentals of Body CT*. 3rd edn. Philadelphia: Elseiver.

Wong MD, Dorr AE, Walls JR, et al. (2012) A novel 3-D mouse embryo atlas based on micro-CT. *Development* **139**, 3248–3256.

Wong MD, Spring S, Henkelman RM (2013) Structural stabilization of tissue for embryo phenotyping using micro-CT with iodine staining. *PLoS ONE* **8**, e84321.

Wong MD, Maezawa Y, Lerch JP, et al. (2014) Automated pipeline for anatomical phenotyping of mouse embryos using micro-CT. *Development* **141**, 2533–2541.

Supporting Information

Additional Supporting Information may be found in the online version of this article:

Table S1. A Microsoft EXCEL file containing the contents of Table 1 along with additional columns of specimen preparation and imaging parameters for readers to manipulate and use for comparing and contrasting various aspects of specimen affinities, sizes, preparation regimes, and μCT imaging.

Table S2. This sample reporting spreadsheet, or a modified version thereof, is intended to be helpful for ensuring the full documentation (and later reporting) of specimen storage, preparation, and CT-scanning parameters at each stage of diceCT imaging research.

Table S3. Comparisons of iodine-based contrast agents with alternatives commonly used in contrast-enhanced μCT imaging.